Lin et al. eLight (2025) 5:6
https://doi.org/10.1186/s43593-025-00083-z

elight.springeropen.com

RESEARCH ARTICLE

Open Access

Pump-induced stimulated superradiant Smith-Purcell radiation with ultra-narrow linewidth

Yuechai Lin[1,2†], Jinyu Li[1,2†], Fang Liu[1,2*†], Weisi Meng[3], Pan Pan[3], Hanqi Feng[1,2], Wei Zhang[1,2], Xue Feng[1,2], Kaiyu Cui[1,2], Jinjun Feng[3] and Yidong Huang[1,2*]

Abstract

Lasers with the gain medium of gas, liquid, semiconductor, and solid could generate coherent light with rather narrow spectral linewidth, which play an important role in the fields of communication, measurement, sensing, and so on. Although free electron lasers have been realized with their unique advantages, they face challenges in narrowing the spectral linewidth, owing to electron energy fluctuation, Coulomb effect, and other mechanism. Here we demonstrate the superradiant Smith-Purcell radiation (S-SPR) in terahertz frequency band with ultra-narrow and continuously tunable linewidth in a compact device. By proposing a new effect of pump-induced stimulated S-SPR (PIS-SPR), the spectral linewidth could be reduced to 0.3 kHz @ 291.7 GHz, which is about two–six orders of magnitude narrower compared with those obtained by accelerators and other electron devices. Meanwhile, the wide range of continuously tunable spectral linewidth spanning 0.3–900 kHz is observed for the first time. This work provides a way to greatly narrow the spectral linewidth of free electron radiation and to achieve high-order harmonic of S-SPR in a compact device, and offers a platform to study the interaction between free electron bunches and different micro-&nano-structures.

1 Introduction

The inventions of masers and lasers, grounded in the concept of stimulated emission [1–3], have yielded highly coherent emissions characterized by extraordinarily narrow spectral linewidths [4]. This has greatly advanced the development of material research [5], optical communications [6, 7], optical fabrications [8, 9], optical sensing [10, 11], etc. Similarly, the interaction between free electrons and the radiated electromagnetic wave gives rise to stimulated free electron emission, such as stimulated Cherenkov radiation [12, 13], Smith-Purcell radiation [14, 15], synchrotron radiation [16, 17], and so on [18, 19], forming the foundation for the development of free electron lasers [20–22]. However, compared with maser and laser, radiations produced by free electrons exhibit notably wide spectral linewidths [4, 23, 24], which is attributed to the three factors, namely the instability of electron kinetic energy, coulomb effect and the finite number of electron bunches [25, 26].

Superradiant Smith-Purcell radiation (S-SPR), produced by a train of electron bunches passing over a periodic grating [27], could generate ultra-narrow spectral linewidth in theory [28, 29], which would be greatly beneficial to applications of imaging, sensing, communication,

†Yuechai Lin, Jinyu Li and Fang Liu are co-first authors.

*Correspondence:
Fang Liu
liu_fang@tsinghua.edu.cn
Yidong Huang
yidonghuang@tsinghua.edu.cn
[1] Department of Electronic Engineering, Tsinghua University, Beijing 100084, China
[2] Tsinghua National Laboratory for Information Science and Technology, Beijing 100084, China
[3] National Key Laboratory of Science and Technology on Vacuum Electronics, Beijing Vacuum Electronics Research Institute, Beijing, China

and et al. Nevertheless, the above-mentioned three factors worsen the radiation linewidth to tens of kHz or even GHz [23, 24, 30–32]. Moreover, the large size of equipment, e.g. accelerators [23, 24, 32], customized setups [27] and orotrons [30, 31], imposed limitations on the applications of S-SPR. Although some previous works had proposed different ways to realize high performance S-SPR [33, 34], ampere-level currents or hundreds-watts of pump power [35] were needed and could hardly be achieved with compact structures.

Here we report the first compact S-SPR device with ultra-narrow and continuously tunable spectral linewidth. By proposing and realizing the new effect of pump-induced stimulated S-SPR (PIS-SPR), the harmonic of S-SPR at the frequency of ~ 0.3 THz is successfully observed and the radiation linewidth could be continuously tuned from 900 kHz to 0.3 kHz. The narrowest linewidth is two–six orders of magnitude narrower than those of previous reported S-SPR. The device size is 22 cm × 7 cm × 6.5 cm and the weight is only 1.68 kg, which can be easily held by one hand.

2 Results

The proposed device with PIS-SPR effect is sketched in Fig. 1a. The free electron beam passes through the three-section vacuum tube, including the electron pre-bunching, electron-compression and harmonic-emission sections. In the first two sections, the copper grating along *z*-axis and Fabry–Perot (F-P) cavity along y-axis help the input THz pump wave generate PIS-SPR, while

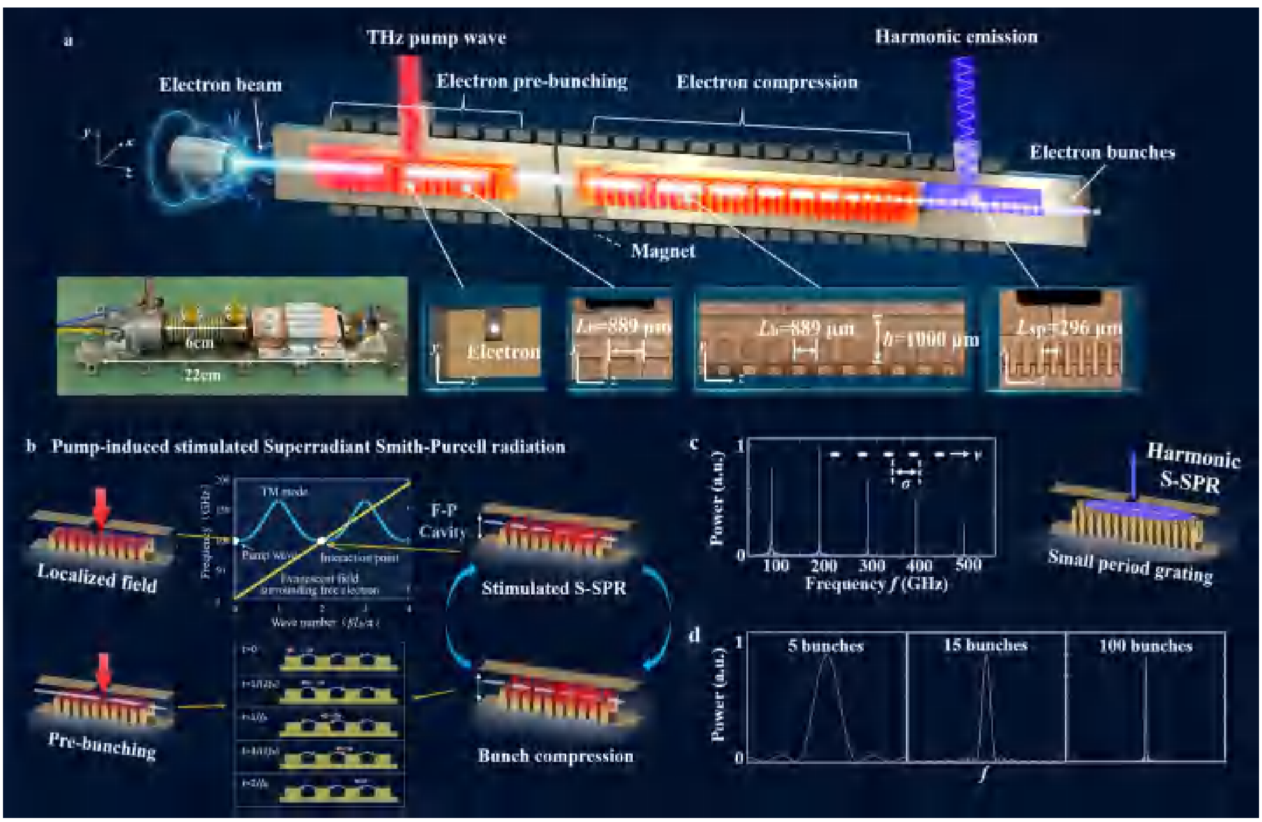

Fig. 1 Pump-induced stimulated superradiant Smith-Purcell radiation (PIS-SPR) and compact device. **a** Schematic view of the THz high-harmonic PIS-SPR device consisting of the electron pre-bunching, electron-compression and harmonic-emission section. Insets illustrate the photos of fabricated device and the details of the copper grating and resonant structure and the detailed dimensions of the PIS-SPR Device are listed in Table 1. **b** Schematic view illustrating the mechanism of PIS-SPR. First, a low-frequency and low-power THz pump wave excites the TM mode in pre-bunching section, corresponding to the left white dot in the dispersion diagram, and forms a localized electromagnetic mode on the gratings; Second, the localized mode pre-bunches the direct-current free electron beam; Third, the bunched electrons interact with the gratings, which corresponds to the right white dot in the dispersion diagram, and generate S-SPR at the same frequency as the pump wave, so that S-SPR resonates in F-P cavity and amplifies the localized mode; Then, the enhanced localized mode further bunches the electrons. The last two steps cycle, producing the PIS-SPR and high-quality bunched electrons. And the bunching process of free electrons by localized mode is depicted schematically. **c** Schematic of harmonics surrounding electron bunches and the grating with small period for harmonic extraction. **d** Schematic of PIS-SPR with different spectrum linewidth excited by different numbers of electron bunches

Table 1 Dimensions of Each Section in the PIS-SPR Device

Section	Dimensions
Electron Pre-Bunching Section	Section Length: ~ 1 cm Grating Pitch: $L_b = 889$ μm F-P Cavity Length: $h = 1000$ μm
Electron-Compression Section	Section Length: ~ 4 cm Grating Pitch: $L_b = 889$ μm F-P Cavity Length: $h = 1000$ μm
Harmonic-Emission Section	Section Length: ~ 0.8 cm Grating Pitch: $L_{sp} = L_b/3 = 296$ μm F-P Cavity Length: $h = 870$ μm
Overall Device	22 cm (L) × 7 cm (W) × 6.5 cm (H)

the last section with small pitch of grating is for extracting the high-order harmonics. The insets illustrate the cross section of the grating in x–y plane, the photos of gratings with different pitches and a full view of the entire device. Further details on the specific components of the device could be found in Supplementary Sects. 2.

Figure 1b illustrates the detailed process of PIS-SPR. The low-frequency and low-power THz pump wave is injected into electron pre-bunching section, exciting the TM mode whose transverse wavenumber along z-axis tends to zero corresponding to the left white dot in the dispersion diagram. The localized electromagnetic (EM) mode on the grating (grating pitch $L_b = 889$ μm) which pre-bunches the electron beam. In the first half of the cycle, a portion of the DC electrons is decelerated by the electric field; in the second half of the cycle, another portion of the electrons is accelerated by the electric field. As the electrons travel through space, the accelerated electrons gradually catch up with the decelerated electrons, squeezing together in space and forming periodic electron bunches at the frequency of pump wave. Subsequently, these pre-bunched electrons fly into the electron compression section and interact with the gratings continuously, generating S-SPR at the same frequency as the pump wave. Due to the vertical resonant mode within the F-P cavity (cavity length h = 1000 μm) along the y-axis corresponding to the right white dot in the dispersion diagram, the generated S-SPR as well as localized EM field can be amplified and enhanced. The localized field in the slit of grating is enhanced by more than 40 times in the electron compression section, while only ~ 3 times in pre-bunching section. Then, the localized EM mode further bunches the electrons. The localized EM mode and the electron bunches are enhanced alternatively and continuously, forming positive feedback until stable state, which leads to the stimulated S-SPR (namely PIS-SPR), as well as well-bunched periodic electrons. The introduction of the novel PIS-SPR effect allows for a significant reduction in the power required for bunching electrons, scaling down from hundreds of watt to tens of mW (see details in Supplementary Sects. 3). Finally, utilizing the small period grating (grating pitch $L_{sp} = L_b/3 = 296$ μm), the ideal electron bunches could generate high harmonic S-SPR with adjustable linewidth by varying the number of bunches (corresponding to the duration time τ of electron beam) as sketched by Fig. 1c and d. To be mentioned, due to PIS-SPR effect, the electron beam can turn into bunches no matter how small the electron current is, which is different from conventional S-SPR using surface wave excited by electron beam to bunch itself [27]. Thus, there is no threshold of current for generating PIS-SPR.

In previous free electron radiation devices and setups, several factors worsened the radiation linewidth. (1) Limited number of electron bunches N_b. Since the linewidth $\Delta\omega \propto 1/N_b$ [28] and N_b in S-SPR was much less in electron accelerators [23, 32], the $\Delta\omega$ is typically larger than GHz [23, 24]. Even with the application of hundreds of bunches and frequency locking, the linewidth $\Delta\omega$ is only decreased to 28 MHz [32]. (2) Cathode voltage fluctuation (electron energy fluctuation). In accelerators, orotrons and backward wave oscillators (BWO), the radiation frequency is intrinsically tied to the electron energy (velocity) which is decided by the cathode voltage [25]. The inevitable fluctuations of voltage would result in the tens of kHz to MHz linewidth [30]. (3) Coulomb repulsion. For high-frequency radiation, the coulomb repulsion expands the electron bunch, leading to the generation of a broader radiation linewidth when the electrons pass over the gratings.

The PIS-SPR device shown in Fig. 1 effectively overcomes the above issues which worsen the linewidth. Based on the effect of PIS-SPR, millions or billions of electron bunches could be generated, cathode voltage fluctuations would have little influence on the pitch of electron bunches, and high power radiation in the device would confine the electrons in bunches against the coulomb repulsion (see detailed simulation and analysis later). The measurement results are illustrated in Fig. 2 by applying a voltage of ~ 23 kV between cathode and anode (V_{ca}) and ~ 48.5 mA current (see measurement setup in Sect. 4 of Supplementary materials). As 100 mW pump wave at frequency of around 97 GHz is input, 3rd harmonic PIS-SPR is observed with maximum output power of 46 mW.

The spectral linewidth of output PIS-SPR with different duration time τ of electron beam (corresponding to the number of electron bunches) is depicted in Fig. 2a. By increasing τ from 1 μs to 10 ms (corresponding the number of electron bunches N_b is increased from ~ 10^5 to ~ 10^9), the spectral linewidth, defined as full width at half maxima (FWHM) of the spectrum, could be tuned from 900 kHz to 0.3 kHz. Compared with previous

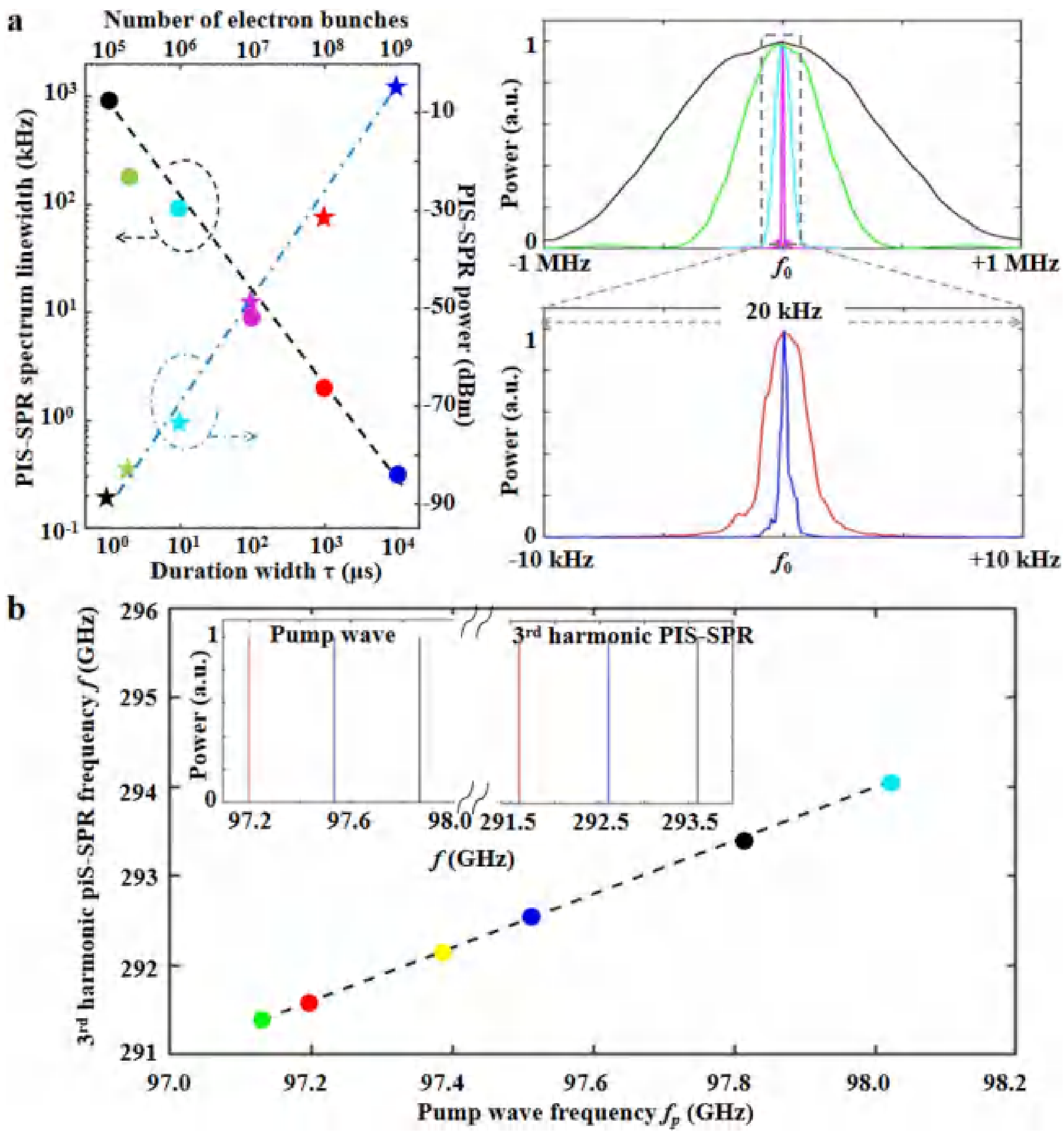

Fig. 2 Measured PIS-SPR frequency and spectral linewidth. **a,** Super-wide continuously tunable spectral linewidth (colored dots) of PIS-SPR from 900 kHz to 0.3 kHz by increasing duration time τ from 1 μs to 10 ms (Corresponding number of electron bunches N_b is increased from ~ 10^5 to ~ 10^9). Insets depict the spectra of PIS-SPR with $\tau = 1$ μs (black), 2 μs (green), 10 μs (cyan), 100 μs (magenta), 1 ms (red) and 10 ms (blue), whose linewidths are 900 kHz, 180 kHz, 90 kHz, 9 kHz, 2 kHz and 0.3 kHz, respectively. The central emission frequency f_0 is 291.684 GHz pumped by 100 mW wave at frequency of 97.228 GHz. The measured power (colored stars) increases with the number of electron bunches, which satisfies with Eq. S3 of S-SPR in Sect. 1 and is discussed in Sect. 7 of Supplementary materials. **b,** The frequency variation of 3rd harmonic PIS-SPR as the pump wave frequency f_p varying from 97.128 GHz to 98.028 GHz. Insets depict the spectrum of pump and 3rd harmonic PIS-SPR wave around 97.5 GHz and 292.5 GHz, respectively

S-SPR generated by the orotrons and electron accelerators [23, 30], the linewidth has been shrunk by about two–six orders of magnitude (see linewidth comparison in Sect. 5 of Supplementary materials), and the wide range of continuously tunable spectral linewidth covering 0.3–900 kHz is observed experimentally for the first time. Actually, theoretically the spectral linewidth could be easily widened to GHz or even wider by shortening τ, while this is limited by the shortest τ of the setup (~ 1 μs) in the experiment. In Fig. 2b, how the frequency of 3rd harmonic radiation follows that of pump wave is illustrated. The triple relationship is strictly satisfied

Table 2 The detailed experiment parameters and data

Voltage (kV) /Current (mA)	Duration time τ	Number of electron bunches N_b	Spectral linewidth	Measured power after attenuation (dBm)
23 kV/48.5 mA	1 µs	9.7×10^4	900 kHz	− 90
	2 µs	1.9×10^5	180 kHz	− 85
	10 µs	9.7×10^5	90 kHz	− 72
	100 µs	9.7×10^6	9 kHz	− 52
	1 ms	9.7×10^7	2 kHz	− 33
	10 ms	9.7×10^8	0.3 kHz	− 9

The measured output power is attenuated for spectrum measurement

between the frequency of PIS-SPR emission and pump wave. Actually, other harmonic frequency with narrow linewidth and stable radiation output could be extracted by varying the pitch L_{sp} of the small period grating in the 3rd section of the device. The emission source of around 0.3 THz with such a narrow linewidth might be applied in the fields, including brain tumor imaging, THz communications, high-precision holographic imaging and terahertz detection. Meanwhile, the radiation power is also measured and depicted as the colored stars in Fig. 2a. With tenfold increase in τ (as well as N_b), the radiation power increases by ~ 20 dBm, that is to say, the increase of radiation power is proportional to N_b [26], satisfying with Eq. S3 of S-SPR (see Sect. 1 and Sect. 7 of Supplementary materials). The detailed experiment parameters and data are concluded in Table 2. Based on the measured variation of linewidth and power of radiation with the number of electron bunches and other factors (see Sect. 7 of Supplementary materials), it can be verified that the narrow linewidth radiation generated here originates from S-SPR. The overall efficiency of the device yields an approximate value of 0.04% considering the energy consumption of electrons and pump wave (see Sect. 4 of Supplementary materials).

3 Discussion

To understand how the stable electron bunches and ultra-narrow linewidth are achieved, numerical simulations of PIS-SPR carried out based on particle-in-cell finite difference time domain. Figure 3a presents the following stages: a periodic localized field with pump wave but without electrons at the beginning (left figure at t1,

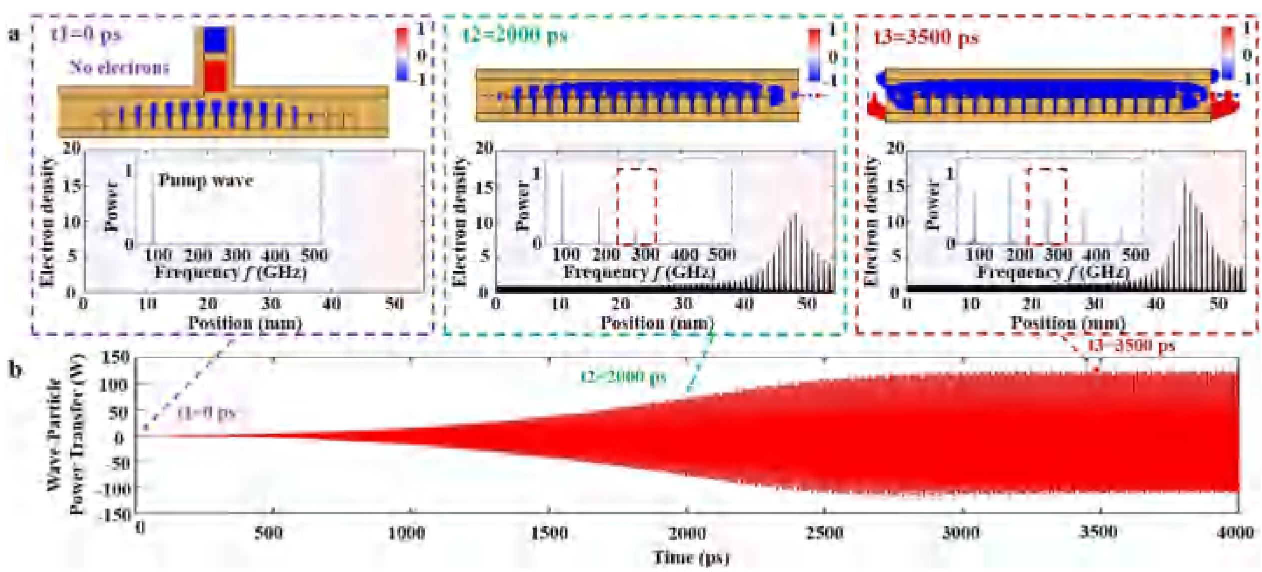

Fig. 3 Simulation the process of PIS-SPR. **a** Electromagnetic field profile, free electron density distribution, and the evanescent field surrounding electrons at time t1 = 0 ps (left), t2 = 2000 ps (middle), and t3 = 3500 ps (right). At t1 = 0, the pump wave excites the localized mode in the electron pre-bunching section of device (the inset shows the spectrum of pump wave); At t2 = 2000 ps, the PIS-SPR results in the amplified EM wave, the bunch of electrons at the frequency of pump wave, and the arise of harmonics of PIS-SPR in the electron-compression section of device (the insets at t2 and t3 shows the spectrum surrounding bunched electrons); At t3 = 3500 ps, the EM wave are very strong, the electrons are well bunched indicated by the electron density, and the intensity of harmonics are comparable with pump wave. **b** Energy exchange between free electrons and electromagnetic wave. The energy of pump wave is enlarged to about 100 W in the device. The purple, green, and red arrows correspond to the three stages in **a**

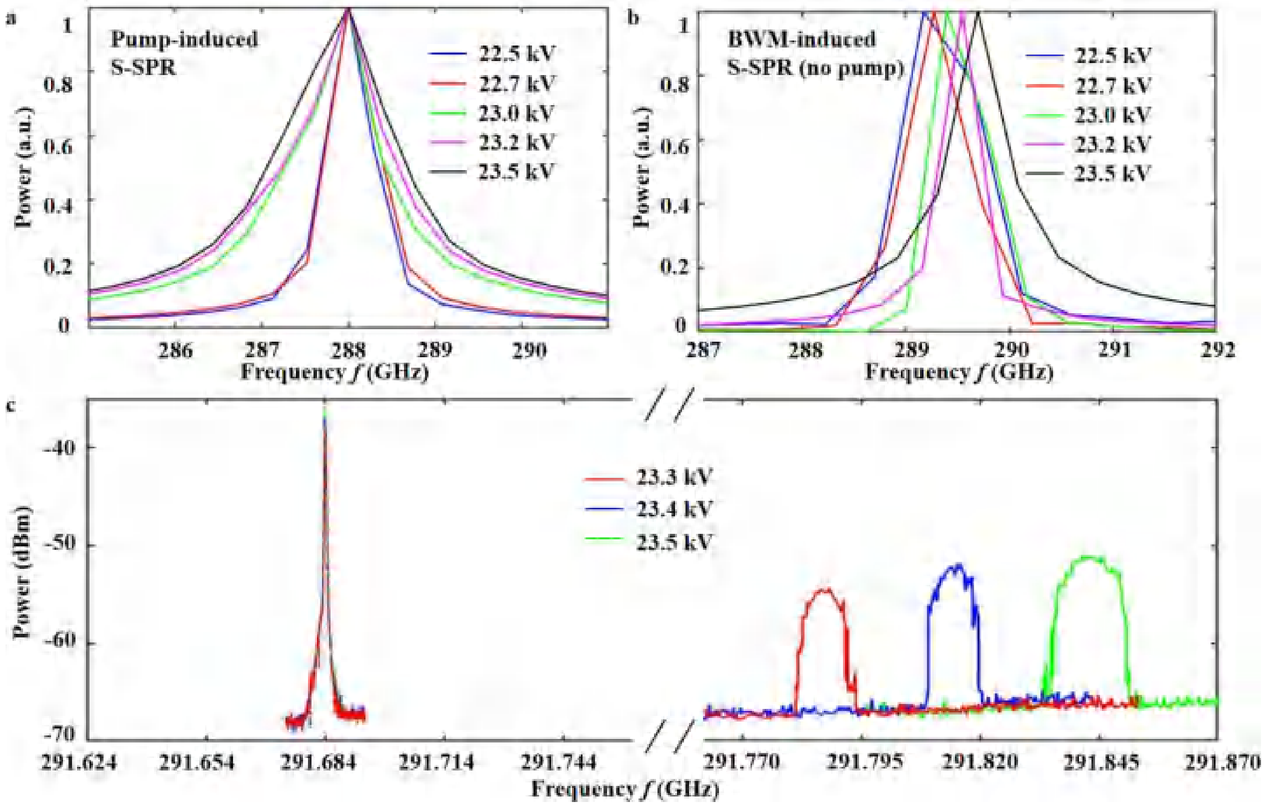

Fig. 4 PIS-SPR eliminate the electron energy fluctuation. **a** Simulated spectra with PIS-SPR effect. The pump wave locks the PIS-SPR at its frequency eliminating the influence of electron energy fluctuation. **b** Simulated spectra of S-SPR induced by backward waveguide mode (BWM). The frequency of S-SPR shifts with electron energy. **c** Measured S-SPR spectra with different electron energy when device is operating under PIS-SPR (left three curves, with pump) and BWM-induced S-SPR (right three curves, without pump). By the way, since the spectral resolution is limited by the software (see Methods), the electron energy fluctuation setting in simulation (500 eV) is larger than that in experiment (100 eV)

the purple arrow in Fig. 3b), an initially amplified wave and bunched electrons (middle figure at t2, the green arrow in Fig. 3b), and a sufficiently amplified pump wave and well-bunched electrons (right figure at t3, the red arrow in Fig. 3b). The harmonics of the evanescent field surrounding the electrons are much stronger as electron density periodically distributed as shown in the bottom figure at t2 and t3. By shrinking the F-P cavity length along y direction and based on the stimulated effect, the power of pump wave for bunching the electrons has been decreased by more than three orders of magnitude compared with open grating structure (see Supplementary Sect. 3). Therefore, the direct-current free electron beam could be transformed to millions, billions or even more electron bunches by the amplified EM wave of hundred-watt power in device and the strong electric field can overcome Coulomb repulsion along the z-axis for confining the electrons in the bunches with size much smaller than the grating pitch. By placing the harmonic emission section at the peak of electron density, the maximum radiation output power can be generated.

Another factor worsening the linewidth, cathode voltage fluctuation (electron energy fluctuation), can also be avoided here. Operating under the mechanism of PIS-SPR as mentioned above, both simulation (Fig. 4a) and measurement results (left curves in Fig. 4c) reveal that the central frequency of PIS-SPR remains fixed even when cathode voltage changes from 22.5 kV to 23.5 kV in simulation and from 23.3 kV to 23.5 kV in experiment (see more simulation results in Supplementary Sect. 6), depending on the dispersion curve and its synchronization with the beam voltage. When no pump wave is injected in the device, the backward waveguide mode (BWM) is excited and oscillates with electron beam, which also generates electron bunches and 3rd harmonic S-SPR (see details in Supplementary Sect. 8). However, indicated by Fig. 4b and right curves in Fig. 4c, the central frequency of BWM induced S-SPR shifts with electron energy. In Fig. 4c, it is obvious that the spectra of PIS-SPR with pump-induced stimulated effect has much narrower linewidth and stronger power compared with those without pump.

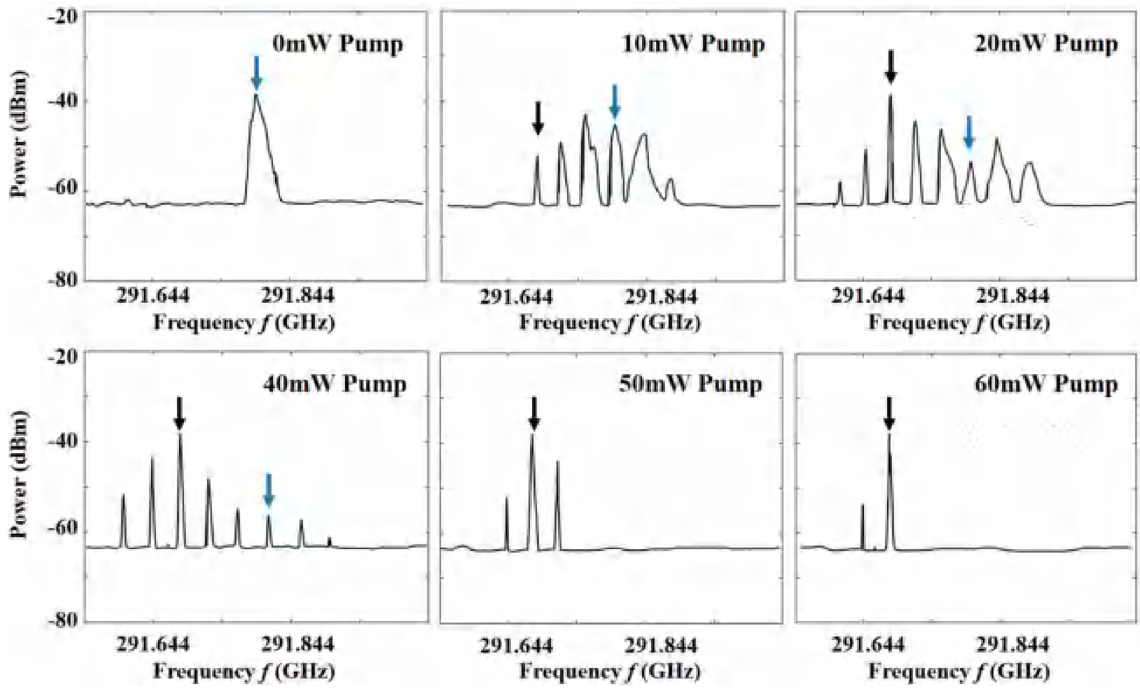

Fig. 5 Measured emission spectra with different pump power. All spectra have the same axis scale, the black arrow indicates the radiation peak of 3rd harmonic of pump wave, and the blue arrow indicates the radiation peak of 3rd harmonic of BWM. Under low pump power, the PIS-SPR effect and BMW-induced SPR exist and compete together. With the increase of pump power, the PIS-SPR gradually dominates the electron bunching process and the peak at 3rd harmonic of BWM is suppressed

The mode evolution of the device from BWM-induced S-SPR to PIS-SPR is studied experimentally by gradually increasing the power of pump wave. Fixing the pump frequency at 97.228 GHz and increasing pump power from 0 to 60 mW, the evolutionary of the emission spectra are measured and shown in Fig. 5. It is evident that, in the absence of a pump wave (0 mW), the electron beam is bunched by the backward wave mode (BWM), as described in Supplementary Sect. 8. Consequently, the emission spectrum features a broad peak at 291.794 GHz (indicated by the blue arrow), with a linewidth on the order of MHz. Therefore, if the objective is to achieve high-power radiation other than a super-narrow linewidth, it is feasible to optimize the structure of the third grating to extract BWM-induced S-SPR.

When pump wave (10 mW, 20 mW and 40 mW) is injected, the free electrons are modulated by both pump wave and BWM wave, resulting in more complicated electron bunching by two frequencies. Besides, the peak at the 3rd harmonic S-SPR by BWM, a narrow peak at the 3rd harmonic emission by PIS-SPR (291.684 GHz, marked by black arrow) and other peaks appear. These peaks form a frequency comb and the frequency interval between any adjacent peaks is equal to the frequency difference of pump wave and BWM. Increasing the power of pump wave, the intensity of 3rd harmonic of pump wave (black arrow) gradually exceeds that of the 3rd harmonic of BWM (blue arrow). The frequency comb should result from the intermodulation distortion and indicate the competition between pump wave and BWM in the device. Furthermore, when the pump power is increased to 50 mW and 60 mW, the PIS-SPR dominates the electron bunching process and the peak at 3rd harmonic of BWM is almost suppressed. Finally, with the injection of 100 mW pump power, only the 3rd harmonic of pump wave remains as stated above. These measured emission spectra clearly reveal the mode evolution from BWM-induced S-SPR to PIS-SPR in the device. By the way, the pump wave power might be reduced by optimizing the parameters, improving fabrication technique [36] or applying a dual-grating structure [37]. If adjusting the pulse width and the duty cycle of beam voltage and power of pump wave, the more complicated electron bunches could be realized for radiation generation and other applications.

By the way, the pre-bunched vacuum devices for linear beam devices are typically klystrode [38] and twystrode [39] using gated thermionic cathodes or field emission cathodes. However, the mechanism, structure, and performance of our device with PIS-SPR are different. PIS-SPR is a novel effect proposed and realized in this paper, which could overcome the three factors worsening the linewidth, while generating electron bunches directly through the electric field modulation of RF signal has rather low-bunching frequency and voltage fluctuation. The PIS-SPR device applies resonant cavities and shows the significant characteristics of S-SPR.

4 Conclusion

As mentioned at the beginning, although the free electron laser had been realized for a long time [21], the radiation spectrum of free electrons could not be as narrow as those of maser or laser [4, 23, 24]. The above results demonstrate the generation of PIS-SPR of 46 mW with ultra-narrow and continuously tunable linewidth at frequency of ~ 291.684 GHz in a compact device. Benefiting from the proposed new PIS-SPR effect, the three factors for worsening spectral linewidth, namely finite number of electron bunches, electron energy fluctuation, and Coulomb repulsion, could be conquered and the linewidth could be as narrow as 0.3 kHz which is about two–six orders of magnitude narrower than that of previous reported S-SPR [23, 30]. By varying the duration time τ of electron beam (the number of electron bunches), the wide-range continuously-tunable spectral linewidth covering 0.3–900 kHz is also observed for the first time, which also provides the way to measure the number of millions to billions of electrons bunches. And the volume of the device is shrunk by about 10 to 10000 times compared with the other S-SPR devices (see Fig. S6 in Supplementary Sects. 5), which is suitable for compact desktop and handhold applications. This work provides the possibilities of not only realizing compact, narrow linewidth radiation sources in different frequency region which would promote the applications of S-SPR in different fields, but also generating frequency-locked/-tunable free electron bunches for interaction with different materials and micro-/nano-structures. And the proposed stimulated effect to enhance the light field might also be considered for on-chip electron acceleration to achieve a higher electron acceleration gradient [40].

5 Materials and methods

5.1 Design of cavity and grating structure

As introduced in the text above, the power of the pump wave is amplified to hundred watt by the stimulated effect. Therefore, the design of cavity length and grating structure is key for achieving a compact device. The pump-excited localized EM field in the grating slits with polarization parallel to the z axis is utilized to modulate the energy of flying electrons. It should be satisfied that the phase of the pump-excited EM mode varies 2π when the electron passes through one pitch of the grating, and hence the electron beam is pre-bunched by the alternative speeding up and slowing down. Then the pre-bunched electrons generate S-SPR at the bunching frequency, as well as the pump frequency, with the direction vertical to the grating. With the F-P cavity, the emitted S-SPR is reflected up and down for enhancing E_z and electron compression. Finally, the above processes result in the stimulated S-SPR in the resonant cavity. The numerical simulation for the above process could be found in the Supplementary Information Sect. 3. It is indicated that with PIS-SPR effect, the power of pump wave for bunching electron beam can be decreased from hundred watt to tens of mW.

5.2 Device fabrication

With oxygen-free copper, the grating and F-P cavity structure are fabricated by ultra-precision machining technology [41]. Then the electron gun, electron collector and vacuum tube are connected by welding technique. A group of periodic permanent magnets with ~ 0.5 T are wrapped around the vacuum tube to ensure the electron beam travel well through the interaction tunnel inside the grating. Finally, the air in the tube is evacuated to achieve a vacuum degree of ~ 10^{-11}mbar. The detailed components of this compact device can be found in the Supplementary Information Sect. 2.

5.3 Measurement setup

Figure S5 shows the measurement setup. The THz pump wave is produced by the signal generator (Ceyear 1465D), and the power amplifier working in the 90–100 GHz can amplify the pump power up to 100mW. The power meter (VDI Erickson PM58) and spectrum analyzer (Agilent 8563E) combined with harmonic mixer are used to measure the radiation power and spectrum. The compact S-SPR device is powered by the customed power supply. The voltage V_{ca} with pulse output can be tuned from 0 to 25kV, the pulse repetition frequency can be changed from 10 Hz to 10 kHz, and the maximum duration time τ for each pulse can achieve 10 ms. As mentioned in the text above, the inevitable cathode voltage fluctuation still exists in the customed power supply, but the radiation spectrum demonstrates the very good stability.

5.4 Numerical simulation

The numerical simulation is conducted in the commercial software CST. The eigenmode solver is used to calculate the dispersion curve and design the structure of grating and F-P cavity. The PIC particle tracking solver is used to simulate the process of harmonic S-SPR, electron bunching, and the interaction between EM field and electrons. It should be mentioned that, due to the limitation of the spectral resolution in software CST, the linewidth in Fig. 4a and b could not be further narrowed.

Supplementary Information

The online version contains supplementary material available at https://doi.org/10.1186/s43593-025-00083-z.

Supplementary Material 1.

Author contributions

F.L. and Y.L. proposed the idea of the research work. F.L., Y.L. and J.L. performed the theoretical analysis. Y.L., J.L. and H.F. performed the numerical simulations. Y.L., J.L., W.M., P.P., H.F., F.L. and J.F fabricated the device and carried out the experiment. K.C., X.F. and W.Z. and Y.H. discussed the results. Y.L., J.L., F.L. and H.F. prepared the paper which was revised by all authors. F.L., J.F. and Y.H. led the overall direction of the project.

Funding

This work was supported by the National Key Research and Development Program of China under Contracts No. 2024YFA1209202, the National Natural Science Foundation of China (Grant No. U22A6004 and No. 62301294) and the Frontier Science Center for Quantum Information.

Availability of data and materials

All data are available from the corresponding authors upon reasonable request. The codes that support the plots within this paper and other findings of this study are available from the corresponding authors upon reasonable request.

Declarations

Competing interests

The authors declare no competing interests.

Received: 3 December 2024 Revised: 24 February 2025 Accepted: 3 March 2025
Published online: 17 April 2025

References

1. A. Einstein, Zur Quantentheorie der Strahlung [On the quantum theory of radiation]. Physikalische Zeitschrift **18**, 121–128 (1917)
2. J.P. Gordon, H.J. Zeiger, C.H. Townes, Molecular microwave oscillator and new hyperfine structure in the microwave spectrum of NH_3. Phys. Rev. **95**, 282–284 (1954)
3. A.L. Schawlow, C.H. Townes, Infrared and optical masers. Phys. Rev. **112**, 1940–1949 (1958)
4. Z.X. Bai et al., A comprehensive review on the development and applications of narrow-linewidth lasers. Microw. Opt. Technol. Lett. **64**, 2244–2255 (2022)
5. D.J. Joe et al., Laser-material interactions for flexible applications. Adv. Mater. **29**, 1606586 (2017)
6. H. Al-Taiy, N. Wenzel, S. Preussler, J. Klinger, T. Schneider, Ultra-narrow linewidth, stable and tunable laser source for optical communication systems and spectroscopy. Opt. Lett. **39**, 5826–5829 (2014)
7. M. Ross et al., Space optical communications with the Nd:YAG laser. Proc. IEEE **66**, 319–344 (1978)
8. R.R. Gattass, E. Mazur, Femtosecond laser micromachining in transparent materials. Nat. Photonics **2**, 219–225 (2008)
9. L. Yang et al., Laser printed microelectronics. Nat. Commun. **14**, 1103 (2023)
10. D.K. Killinger, N. Menyuk, Laser remote-sensing of the atmosphere. Science **235**, 37–45 (1987)
11. M. Hosseini, G. Guccione, H.J. Slatyer, B.C. Buchler, P.K. Lam, Multimode laser cooling and ultra-high sensitivity force sensing with nanowires. Nat. Commun. **5**, 4663 (2014)
12. P.A. Cherenkov, Visible light from clear liquids under the action of gamma radiation. Comptes Rendus de l'Académie des Sciences de l'URSS **2**, 451–454 (1934)
13. F. Liu et al., Integrated Cherenkov radiation emitter eliminating the electron velocity threshold. Nat. Photonics **11**, 289–292 (2017)
14. G. Doucas, J.H. Mulvey, M. Omori, J. Walsh, M.F. Kimmitt, First observation of Smith-Purcell radiation from relativistic electrons. Phys. Rev. Lett. **69**, 1761–1764 (1992)
15. S.J. Smith, E.M. Purcell, Visible light from localized surface charges moving across a grating. Phys. Rev. **92**, 1069 (1953)
16. F.R. Elder, R.V. Langmuir, H.C. Pollock, Radiation from electrons accelerated in a synchrotron. Phys. Rev. **74**, 52–56 (1948)
17. T. Nakazato et al., Observation of coherent synchrotron radiation. Phys. Rev. Lett. **63**, 1245–1248 (1989)
18. D.F. Alferov, A.B. Yu, P.A. Cherenkov, Radiation from relativistic electrons in a magnetic undulator. Soviet Physics Uspekhi **32**, 200 (1989)
19. H. Boersch, C. Radeloff, G. Sauerbrey, Experimental detection of transition radiation. Phys. Rev. Lett. **7**, 52 (1961)
20. L.R. Elias, W.M. Fairbank, J.M.J. Madey, H.A. Schwettman, T.I. Smith, Observation of stimulated emission of radiation by relativistic electrons in a spatially periodic transverse magnetic-field. Phys. Rev. Lett. **36**, 717–720 (1976)
21. D.A.G. Deacon et al., First operation of a free-electron laser. Phys. Rev. Lett. **38**, 892–894 (1977)
22. P. Emma et al., First lasing and operation of an angstrom-wavelength free-electron laser. Nat. Photonics **4**, 641–647 (2010)
23. Y.F. Liang et al., Observation of coherent Smith-Purcell and transition radiation driven by single bunch and micro-bunched electron beams. Appl. Phys. Lett. **112**, 053501 (2018)
24. A. Aryshev et al., Monochromaticity of coherent Smith-Purcell radiation from finite size grating. Phys. Rev. Accel. Beams **20**, 024701 (2017)
25. J.C. Gallardo, L. Elias, G. Dattoli, A. Renieri, Instability in a multimode free-electron laser—effects of electron-energy drift. Phys. Rev. A **34**, 3088–3100 (1986)
26. K.J. Kim, Spectral bandwidth in free-electron-laser oscillators. Phys. Rev. Lett. **66**, 2746–2749 (1991)
27. J. Urata et al., Superradiant Smith-Purcell emission. Phys. Rev. Lett. **80**, 516–519 (1998)
28. B.E. Billinghurst et al., Observation of superradiant synchrotron radiation in the terahertz region. Phys. Rev. Spec. Top. Accel Beams **16**, 060702 (2013)
29. D.Y. Sergeeva, A.P. Potylitsyn, A.A. Tishchenko, M.N. Strikhanov, Smith-Purcell radiation from periodic beams. Opt. Express **25**, 26310–26328 (2017)
30. B.S. Dumesh, V.P. Kostromin, F.S. Rusin, L.A. Surin, Highly sensitive millimeter-wave spectrometer based on an orotron. Meas. Sci. Technol. **3**, 873–878 (1992)
31. Y.A. Grishin et al., Pulsed orotron—a new microwave source for submillimeter pulse high-field electron paramagnetic resonance spectroscopy. Rev. Sci. Instrum. **75**, 2926–2936 (2004)
32. S.E. Korbly, A.S. Kesar, J.R. Sirigiri, R.J. Temkin, Observation of frequency-locked coherent terahertz Smith-Purcell radiation. Phys. Rev. Lett. **94**, 054803 (2005)
33. Y.X. Zhang, L. Dong, Enhanced coherent terahertz Smith-Purcell superradiation excited by two electron-beams. Opt. Express **20**, 22627–22635 (2012)
34. Y.C. Zhou, Y.X. Zhang, S.G. Liu, Electron-beam-driven enhanced terahertz coherent Smith-Purcell radiation within a cylindrical quasi-optical cavity. IEEE Trans. Terahertz Sci. Technol. **6**, 262–267 (2016)
35. Z.J. Shi et al., Coherent terahertz Smith-Purcell radiation from beam bunching. Nucl. Instrum. Methods Phys. Res. Sect. A **578**, 543–547 (2007)
36. A.M. Cook et al., Demonstration of a high power, wideband 220-GHz traveling wave amplifier fabricated by UV-LIGA. IEEE Trans. Electron Devices **61**, 43–49 (2014)
37. X. Xing et al., Enhanced coherent THz radiation by dual groove grating Smith-Purcell effect. *2020 45th International Conference on Infrared, Millimeter, and Terahertz Waves (IRMMW-THz)*, 1–2. (2020)

38. K. Nguyen et al., Analysis of the 425-MHz klystrode. IEEE Trans. Electron Devices **38**, 2212–2220 (1991)
39. M. Garven et al., Characterization of field emitter arrays (FEAs) for a twystrode amplifier. *1997 IEEE International Conference on Plasma Science*. 283 (1997)
40. N.V. Sapra et al., On-chip integrated laser-driven particle accelerator. Science **367**, 79–83 (2020)
41. P. Pan et al., *Demonstration of a 263-GHz traveling wave tube for electron paramagnetic resonance spectroscopy. IEEE Transactions on Electron Devices* (Advance online publication, New York City, 2023)